A Reliable Approach for Modeling the Actual Antenna Pattern in Millimeter-Wave Communication

Fulvio Babich and Massimiliano Comisso

***Abstract*—This letter presents a mathematical framework for evaluating the link capacity of an interfered communication link in a millimeter-wave mobile scenario, accounting in detail for the shape of the antenna pattern and for the statistic of the direction of arrivals. The developed approach, whose accuracy is verified by Monte Carlo validations in 2D and 3D wireless environments, does not require simplified antenna models, thus enabling to maintain the actual pattern during the analysis.**

***Index Terms*—Millimeter-wave communication, antenna radiation pattern, interference, direction of arrival, link capacity.**

I. Introduction

THE growing interest towards millimeter-wave (mmWave) technology has lead to the development of several proposals [1]–[8], for analyzing and improving the functionalities enabled by the IEEE 802.15.3c and 802.11ad standards [9], [10]. Within these proposals, the antenna pattern plays a fundamental role, since the small size of the radiating elements operating in the 60 GHz band has made feasible the use of antenna arrays on the communication devices, thus enabling spatial reuse by beamforming operations [11]. However, to maintain the analytical tractability of a considered problem, the pattern shape is often simplified. The most common pattern approximations adopt circular sectors [1], infinitesimal beamwidths [2], flat-topped geometries [3]–[5], and directional models [6]–[8].

These approximations idealize many aspects of a real pattern, whose shape may be in general much more complex than that assumed in the commonly adopted simplified models. In fact, this shape may include transition zones and ripples in the main lobe, grating and secondary lobes, and narrow or large null regions [12]. The difference between ideal and actual pattern may introduce considerable discrepancies between theoretical and practical results. Therefore, a more realistic pattern may be introduced to improve the reliability of the analysis. This adoption however makes difficult to derive closed-form expressions for an investigated link quality metric, such as, for example, the success probability. Thus, a modeling strategy capable to guarantee the analytical tractability of a considered problem maintaining the actual shape of the pattern during the analysis may represent a desirable advance.

To deal with this issue, this letter proposes a theoretical approach for an accurate modeling of the antenna pattern in 2D and 3D scenarios. The approach is applied to a problem of link capacity estimation in an interfered multipath-fading environment. Monte Carlo validations are used to verify the accuracy of the developed framework, which furthermore provides, in some specific cases, expressions available in analytical form.

The letter is organized as follows. Section II introduces the network scenario. Section III presents the pattern modeling approach and the capacity analysis. Section IV discusses the numerical results. Section V summarizes the main conclusions.

Manuscript received April 1, 2015; revised June 12, 2015; accepted June 12, 2015. The associate editor coordinating the review of this paper and approving it for publication was T. Yioultsis.

The authors are with the Dipartimento di Ingegneria e Architettura (DIA), University of Trieste, 34100 Trieste, Italy (e-mail: mcomisso@units.it).

Digital Object Identifier 10.1109/LCOMM.2015.2445764

II. Scenario

Consider a wireless network in which a destination D is located at the center O of a ball $B_\nu(O,\bar{R})$ of radius $\bar{R}$ and dimension $\nu \in \{2,3\}$. This destination communicates with its desired source S lying at a distance $\hat{R}(\leq \bar{R})$ in the presence of L interferers uniformly distributed in $B_\nu(O,\bar{R})$, that is, on a disk for $\nu = 2$, and in a ball for $\nu = 3$. Accordingly, the cumulative density function (cdf) of the distance R_l between D and the l-th interferer may be expressed as [13]:

$$F_{R_l}(r_l) = \frac{1}{\bar{R}^\nu} \begin{cases} 0 & r_l < 0 \\ r_l^\nu & 0 \leq r_l \leq \bar{R} \\ \bar{R}^\nu & r_l > \bar{R} \end{cases} \tag{1}$$

In reception, D adopts a normalized antenna power gain pattern $\mathcal{P}(\omega)$, which is obtained from a broadside array and where the direction ω is the azimuth angle $\phi \in \mathbf{\Omega}_2 = [0, 2\pi)$ for $\nu = 2$, and the zenith-azimuth pair $(\theta, \phi) \in \mathbf{\Omega}_3 = [0,\pi] \times [0, 2\pi)$ for $\nu = 3$. In particular, a uniform linear array (ULA) of N elements lying on the x-axis is adopted for $\nu = 2$, while a uniform square array (USA) of $N \times N$ elements lying on the $x - z$ plane is adopted for $\nu = 3$. Thus, to jointly model the 2D and 3D cases, $\mathcal{P}(\omega)$ may be represented by [12]:

$$\mathcal{P}(\omega) = \prod_{j=1}^{\nu-1} \left| \frac{\sin\left[N\pi d S_j^{(\nu)}(\omega)\right]}{N \sin\left[\pi d S_j^{(\nu)}(\omega)\right]} \right|^2, \tag{2}$$

where d is the inter-element distance expressed as a multiple of the carrier wavelength λ, and:

$$S_j^{(\nu)}(\omega) = \begin{cases} \cos\phi & j = 1, \nu = 2 \\ \sin\theta\cos\phi & j = 1, \nu = 3 \\ \cos\theta & j = 2, \nu = 3 \end{cases} \tag{3}$$

The propagation channel is characterized by path-loss attenuation and multipath-fading. More precisely, the path-loss function is:

$$\varrho(r_l) = (r_l^\alpha + \epsilon)^{-1}, \tag{4}$$

where $\alpha(> 2)$ is the path-loss exponent and ϵ is a nonnegative parameter that identifies a classic unbounded path-loss model for $\epsilon = 0$ and a bounded path-loss model for $\epsilon > 0$. For each source (desired or interfering), a probability density function (pdf) $f_Q(q)$ models the power fluctuation Q due to fading, and another pdf $f_{\Omega'}(\omega')$ models the spreading of the direction of arrival (DOA) Ω' due to multipath. More precisely, $f_{\Omega'}(\omega')$ is selected as a Laplacian distribution, whose reliability in describing the spatial channel has been assessed by several measurement campaigns [14]. Hence, the pdf of the DOA may be expressed for $\nu \in \{2, 3\}$ as [14]:

$$f_{\Omega'}(\omega') = \begin{cases} K_\nu \exp\left(-\left|\rho^{(\nu)}(\omega')\right|\right) & \omega' \in \mathbf{\Omega}_\nu \\ 0 & \text{otherwise} \end{cases} \tag{5}$$

where K_ν is a normalization constant, and:

$$\rho^{(\nu)}(\omega') = \left(\frac{2}{\sigma^2}\right)^{\frac{\nu-1}{2}} \cdot \begin{cases} \phi - \pi & \nu = 2 \\ (\theta - \pi/2)(\phi - \pi) & \nu = 3 \end{cases} \tag{6}$$

with σ denoting the angular spread. For $\nu = 3$, (5) is modeled as the product of two univariate Laplacian pdfs, thus assuming, as in [14], the separability of the zenith and azimuth statistics.

III. Analysis

The analysis of the described scenario requires two steps. The first one provides a probability mass function (pmf) of an equivalent gain that jointly models $\mathcal{P}(\omega)$ and $f_{\Omega'}(\omega')$. The second step provides a parametric family of link capacity values, each obtained for a given gain, which are subsequently weighed according to the pmf, so as to evaluate the overall link capacity by applying the concept of mixture distribution [15].

A. Pattern-DOA Statistic Modeling

As a first step, one has to derive the equivalent pattern [16]:

$$g(\omega) = \int_{\mathbf{\Omega}_\nu} \mathcal{P}(\omega') f_{\Omega'}(\omega' - \omega) \mathrm{d}\omega', \tag{7}$$

which enables to jointly account for the receiving pattern and the DOA statistic within a unique function by averaging each value of $\mathcal{P}(\omega)$ over the pdf $f_{\Omega'}(\omega')$. Since ω is the realization of a random variable (r.v.) Ω, also the equivalent gain may be viewed as a r.v. G. In general, $\mathcal{P}(\omega)$, and hence $g(\omega)$, are not invertible functions of ω, thus the statistic of G cannot be derived in closed-form, and an approximated strategy must be developed. To this aim, one may recall that $\mathcal{P}(\omega)$ is a normalized pattern and that $f_{\Omega'}(\omega')$ is a pdf, thus the values of $g(\omega)$ belong to the interval [0, 1]. This interval may be subdivided into $M-1$ adjacent subintervals of equal length $\chi = 1/(M-1)$, to obtain the set of points $\mathbf{G} = \{g_i : g_i = (i-1)\chi,\ i = 1, \ldots, M\}$. The number of directions towards which the equivalent gain is equal to g_i may be evaluated as $\#(\mathbf{\Xi}_i)$, which denotes the cardinality of the set $\mathbf{\Xi}_i = \{\omega : g(\omega) = g_i\}$. Therefore, observing that $\mathbf{\Xi}_1, \ldots, \mathbf{\Xi}_M$ is a sequence of disjoint sets, the pmf of G may be estimated as:

$$f_G(g_i) = \frac{\#(\mathbf{\Xi}_i)}{\sum_{i=1}^{M} \#(\mathbf{\Xi}_i)}, \quad g_i \in \mathbf{G}. \tag{8}$$

The proposed pattern modeling approach has the considerable advantage of modeling $\mathcal{P}(\omega)$ and $f_{\Omega'}(\omega')$ by a unique r.v., whose accuracy in describing $g(\omega)$ may be controlled through the number of gain samples M, which may be increased to allow a more reliable modeling of the actual statistic of $g(\omega)$.

B. Link Capacity

Once the pmf of $g(\omega)$ is available, the interference analysis may be carried out for a given value g_i, that is, assuming the equivalent gain as constant. To this purpose, using (4), the power received by the destination D from the l-th interferer for a gain g_i in absence of mobility may be expressed as:

$$T_l = k g_i \varrho(R_l) = k g_i \left(R_l^\alpha + \epsilon\right)^{-1}, \tag{9}$$

where k is a constant accounting for the height of the antennas and for the transmission power (assumed equal for all sources). The cdf of T_l for a given g_i may be evaluated by inverting (9) with respect to R_l and using (1), thus obtaining:

$$F_{T_l}(t_l; g_i) = \begin{cases} 0 & t_l < g_i\varsigma_1 \\ 1 - \frac{1}{\bar{R}^\nu}\left(\frac{kg_i}{t_l} - \epsilon\right)^\beta & g_i\varsigma_1 \le t_l \le g_i\varsigma_2 \\ 1 & t_l > g_i\varsigma_2 \end{cases} \tag{10}$$

where $\beta = \nu/\alpha$, $\varsigma_1 = k\varrho(\bar{R})$, and $\varsigma_2 = k\varrho(0)$. Recalling that $f_Q(q)$ is the pdf of Q that models the fading effects, the cdf of $P_l = T_l Q$ may be derived from the product distribution [13]:

$$F_{P_l}(p_l; g_i) = \int_0^{+\infty} f_Q(q) F_{T_l}\left(\frac{p_l}{q}; g_i\right) \mathrm{d}q, \tag{11}$$

which can be exploited to obtain the statistic of the total interference I. Usually, the pdf of I cannot be evaluated in closed-form, and hence approximations based on the nearest interferers have been introduced [2], [3]. In particular, according to [2], I may be usefully approximated by:

$$I = \sum_{l=1}^{L} P_l \approx H_L^{(1/\beta)} \max\{P_1, \ldots, P_L\}, \tag{12}$$

where $H_L^{(1/\beta)} = \sum_{l=1}^{L} l^{-1/\beta}$ is the generalized harmonic number of order L in power $1/\beta$. Using the relationship for the scaling of r.v.s [13], the cdf and the pdf of I for a given g_i may be hence calculated, respectively, from:

$$F_I(p; g_i, L) \cong \left[F_{P_l}\left(\frac{p}{H_L^{(1/\beta)}}; g_i\right)\right]^L, \tag{13}$$

$$f_I(p; g_i, L) = \frac{\mathrm{d}F_I}{\mathrm{d}p}. \tag{14}$$

Recalling that $\hat{R}$ denotes the S-D distance and that the maximum of $g(\omega)$ is steered towards S, the desired signal power may be expressed as $\Delta = \hat{t}Q$, where $\hat{t} = k\max\{g(\omega)\}\varrho(\hat{R})$. Hence, the corresponding pdf is $f_\Delta(\delta) = f_Q(\delta/\hat{t})/\hat{t}$. This latter statistic enables to obtain the cdf of the signal-to interference ratio (SIR) $\Upsilon = \Delta/I$ from the ratio distribution [13]:

$$F_\Upsilon(\upsilon; g_i, L) = 1 - \frac{1}{\hat{t}} \int_0^{+\infty} f_Q\left(\frac{\delta}{\hat{t}}\right) F_I\left(\frac{\delta}{\upsilon}; g_i, L\right) \mathrm{d}\delta. \tag{15}$$

The result of the S-D communication may be then established adopting a SIR threshold ψ that accounts for modulation, coding, packet length, and required packet error rate [4], [8]. Thus, the capture probability for a given g_i is evaluated as:

$$\eta(\psi; g_i, L) = \Pr\{\upsilon > \psi\} = 1 - F_\Upsilon(\psi; g_i, L). \tag{16}$$

It is interesting to observe that, in the presence of Rayleigh fading, the pdf of I and the capture probability for $L = 1$ may be represented in analytical form. To this aim, evaluating (11) for $f_Q(q) = e^{-q}u(q)$, where $u(\cdot)$ is the Heaviside step function with $u(0) = 0$, the cdf of P_l may be derived as:

$$F_{P_l}(p_l; g_i) = \int_{\frac{p_l}{g_i\varsigma_2}}^{\frac{p_l}{g_i\varsigma_1}} e^{-q}\left[1-\frac{1}{\bar{R}^\nu}\left(\frac{kg_i q}{p_l}-\epsilon\right)^\beta\right]\mathrm{d}q + \int_{0}^{\frac{p_l}{g_i\varsigma_2}} e^{-q}\mathrm{d}q, \tag{17}$$

which, recalling that $\varsigma_1 = k/(\bar{R}^\alpha + \epsilon)$ and $\varsigma_2 = k/\epsilon$, provides (18), shown at the bottom of the page, where $\gamma(\cdot,\cdot)$ is the lower incomplete gamma function [17]. Now, using (18) in (13)–(16), one may then obtain $f_I(p; g_i, L)$ in (19) and $\eta(\psi; g_i, 1)$ in (20), also, shown at the bottom of the page, where $\zeta_{L,\beta} = kH_L^{(1/\beta)}$ and ${}_2F_1(\cdot,\cdot;\cdot;\cdot)$ is the hypergeometric function [17].

The capacity of the S-D link may be finally evaluated. To this purpose, the parametric family $\eta(\psi; g_i, L)$, resulting for $i = 1, \dots, M$, is employed to derive the capture probability from the mixture distribution [15]:

$$\eta(\psi; L) = \sum_{i=1}^{M} \eta(\psi; g_i, L) f_G(g_i). \tag{21}$$

This latter expression may be used to estimate the limiting performance of the interfered link according to the Shannon bound, thus obtaining the link capacity as:

$$C(\psi; L) = \eta(\psi; L)\log_2(1+\psi). \tag{22}$$

It is useful to notice that the proposed pattern modeling approach allows one to account for the impact of $\mathcal{P}(\omega)$ and $f_{\Omega'}(\omega')$ not only on the link capacity, but on any quantity for which a parametric family of pdfs or cdfs has been calculated during the analysis. For example, one may evaluate, again from the mixture distribution, the pdf of the interference power as:

$$f_I(p; L) = \sum_{i=1}^{M} f_I(p; g_i, L) f_G(g_i). \tag{23}$$

Observe that the expressions in (21)–(23) together with those in (18)–(20) represent a significant result, since, even if the latter ones may seem formally elaborated, they have two relevant advantages that are uncommonly present at the same time in theoretical mmWave modeling: the maintenance of the actual pattern as it is, and the availability of analytical forms.

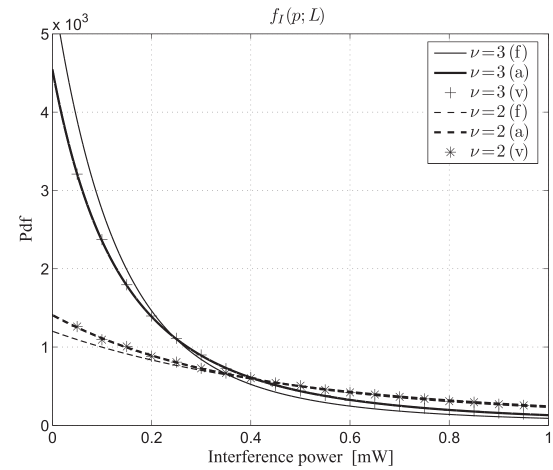

Fig. 1. Pdf of the interference in 2D and 3D cases for $\bar{R} = 2\hat{R} = 10$ m, $\epsilon = 1$, $L = 1$ (f: flat-topped pattern, a: actual pattern, v: Monte Carlo validation).

IV. Results

The results are evaluated for $N = 4$, $d = 1/4$, $\alpha = 3$, $\sigma = \pi/3$, $\chi = 0.01$, $k = 1$ in a Rayleigh fading scenario, and are verified by Monte Carlo validations. Each analytical curve obtained from the actual pattern is compared with that obtained from a flat-topped pattern [3]–[5], in order to check the sensitivity of the results on the actual pattern details. According to the typical rules adopted to derive the flat-topped model of a given pattern, the flat-topped pattern is generated so as to have the main lobe width equal to the half-power beamwidth $\Omega_{3\mathrm{dB}}$ of the actual pattern, the main lobe gain equal to the mean gain of the actual pattern inside $\Omega_{3\mathrm{dB}}$, and the back-lobe gain equal to the mean gain of the actual pattern outside $\Omega_{3\mathrm{dB}}$.

Figs. 1 and 2 report the pdf of the interference power and the link capacity, respectively, for $\bar{R} = 2\hat{R} = 10$ m, $\epsilon = 1$, $L = 1$. The figures refer to the 2D case for a ULA of $N = 4$ elements, and to the 3D case for a USA of $N \times N = 4 \times 4$ elements. The significant matching between the analysis obtained from the actual pattern and the validation confirms the accuracy of the developed framework. Furthermore, this matching reveals that the characteristics of the actual pattern not included in its flat-topped model may have, mainly in the 3D case, a not negligible influence on the final results. This aspect is confirmed by Fig. 3, which is obtained for $\nu = 3$, $\bar{R} = 2\hat{R} = 10$ m, $\epsilon = 1$, and different L values, and by Fig. 4, which is obtained for $\nu = 3$, $\bar{R} = 2\hat{R} = 1$ m, $L = 1$, and different ϵ values. With reference to this latter figure, which shows the critical impact of the

$$F_{P_l}(p_l; g_i) = \left\{1-\exp\left(-\frac{\epsilon p}{kg_i}\right)\left[\exp\left(-\frac{\bar{R}^\alpha p}{kg_i}\right)+\left(\frac{kg_i}{\bar{R}^\alpha p}\right)^\beta \gamma\left(1+\beta, \frac{\bar{R}^\alpha p}{kg_i}\right)\right]\right\} u(p_l) \tag{18}$$

$$f_I(p; g_i, L) \cong F_{P_l}^{L-1}\left(\frac{kp}{\zeta_{L,\beta}}; g_i\right)\exp\left(-\frac{\epsilon p}{g_i\zeta_{L,\beta}}\right)\left[\exp\left(-\frac{\bar{R}^\alpha p}{g_i\zeta_{L,\beta}}\right)\frac{\epsilon L}{g_i\zeta_{L,\beta}} + \frac{L\left(g_i\beta\zeta_{L,\beta}+\epsilon p\right)}{\left(g_i\zeta_{L,\beta}\right)^{1-\beta} p^{1+\beta}\bar{R}^\nu}\gamma\left(1+\beta, \frac{\bar{R}^\alpha p}{g_i\zeta_{L,\beta}}\right)\right] u(p) \tag{19}$$

$$\eta(\psi; g_i, 1) = \begin{cases} 1-\beta k g_i\psi\left[\frac{\pi(\epsilon\hat{t}+kg_i\psi)^{\beta-1}}{\hat{t}^\beta\bar{R}^\nu\sin(\beta\pi)} - \frac{1}{(1-\beta)\hat{t}\bar{R}^\alpha}\,{}_2F_1\left(1, 1-\beta; 2-\beta; -\frac{\epsilon\hat{t}+kg_i\psi}{\hat{t}\bar{R}^\alpha}\right)\right] & 0<\beta<3/2,\ \beta\neq 1 \\ 1-\frac{kg_i\psi}{\hat{t}\bar{R}^\alpha}\log\left(1+\frac{\hat{t}\bar{R}^\alpha}{\epsilon\hat{t}+kg_i\psi}\right) & \beta = 1 \end{cases} \tag{20}$$

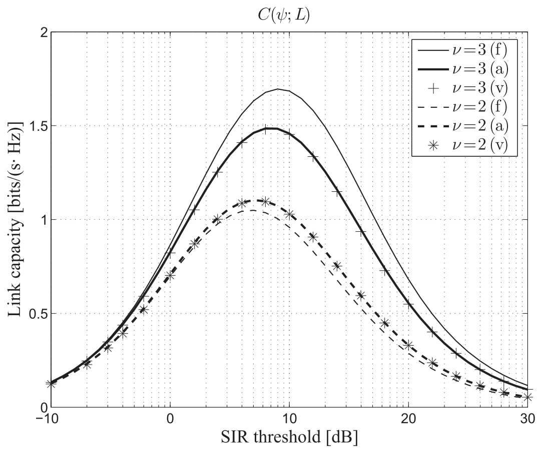

Fig. 2. Link capacity in 2D and 3D cases for $\bar{R} = 2\hat{R} = 10$ m, $\epsilon = 1$, $L = 1$ (f: flat-topped pattern, a: actual pattern, v: Monte Carlo validation).

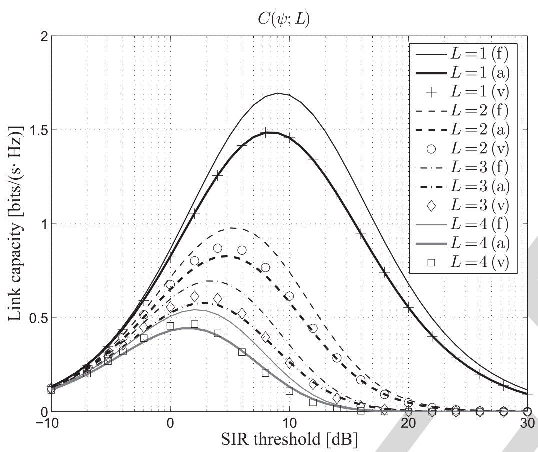

Fig. 3. Link capacity in 3D case for $\bar{R} = 2\hat{R} = 10$ m, $\epsilon = 1$, and different L values (f: flat-topped pattern, a: actual pattern, v: Monte Carlo validation).

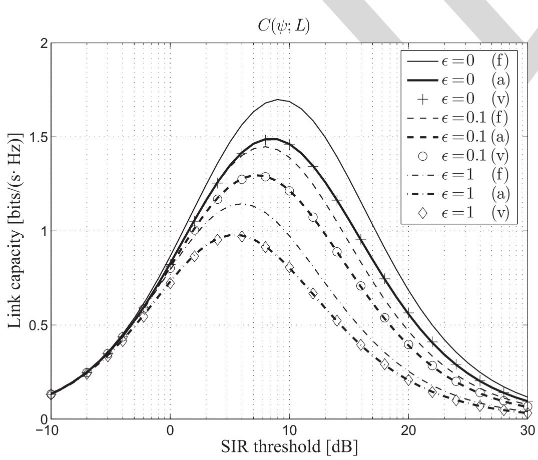

Fig. 4. Link capacity in 3D case for $\bar{R} = 2\hat{R} = 1$ m, $L = 1$, and different ϵ values (f: flat-topped pattern, a: actual pattern, v: Monte Carlo validation).

path-loss model in a short-range scenario, it is worth to notice that the far-field assumption is satisfied. In fact, considering half-wavelength radiators and $d = 1/4$, the maximum dimension of the adopted USA of $N \times N$ elements is $D = \sqrt{2}[N\lambda/2 + (N-1)\lambda/4]$, with $\lambda = 5$ mm at 60 GHz. Thus, since the far-field region begins at $2D^2/\lambda \cong 15$ cm [12], the far-field assumption may be considered satisfied. In summary, the presented results suggest that the proposed approach, combining the concepts of equivalent pattern and mixture distribution, may represent a useful support for the analysis of some scenarios in which, even in the presence of other relevant phenomena, such as interference, path-loss attenuation, and multipath-fading, an investigated link quality metric turns out to be sensitive to the actual pattern details.

V. Conclusion

A mathematical approach for modeling the DOA statistic and the antenna pattern in 2D and 3D mmWave scenarios has been presented and exploited to derive the link capacity in an interfered multipath-fading environment. Monte Carlo validations have confirmed the accuracy of the developed method, which enables to properly account for the actual pattern shape, and, in some specific cases, provides analytical expressions for the investigated performance figures.

References

[1] Q. Chen, J. Tang, D. T. C. Wong, X. Peng, and Y. Zhang, "Directional cooperative MAC protocol design and performance analysis for IEEE 802.11ad WLANs," *IEEE Trans. Veh. Technol.*, vol. 62, no. 6, pp. 2667–2677, Jul. 2013.

[2] F. Babich and M. Comisso, "Capture analysis of mobile multi-packet networks adopting spatial reuse: An alternative study," in *Proc. IEEE GLOBECOM*, 2014, pp. 3477–3482.

[3] A. M. Hunter, J. G. Andrews, and S. Weber, "Transmission capacity of ad hoc networks with spatial diversity," *IEEE Trans. Wireless Commun.*, vol. 7, no. 12, pp. 5058–5071, Dec. 2008.

[4] T. Bai and R. W. Heath, Jr., "Coverage and rate analysis for millimeter-wave cellular networks," *IEEE Trans. Wireless Commun.*, vol. 14, no. 2, pp. 1100–1114, Feb. 2015.

[5] M. Kim, S.-E. Hong, and J. Kim, "Analysis of directional communication via relaying devices in mmWave WPANs," *IEEE Commun. Lett.*, vol. 16, no. 3, pp. 342–345, Mar. 2012.

[6] Y. Wang, X. Kang, H. K. Garg, M. Motani, and Q. Chen, "Throughput maximization for 60 GHz WPANs via device cooperation," *IEEE Commun. Lett.*, vol. 18, no. 5, pp. 785–788, May 2014.

[7] C.-S. Sum and H. Harada, "Scalable heuristic STDMA scheduling scheme for practical multi-Gbps millimeter-wave WPAN and WLAN systems," *IEEE Trans. Wireless Commun.*, vol. 11, no. 7, pp. 2658–2669, Jul. 2012.

[8] S. Singh, R. Mudumbai, and U. Madhow, "Interference analysis for highly directional 60-GHz mesh networks: The case for rethinking medium access control," *IEEE/ACM Trans. Netw.*, vol. 19, no. 5, pp. 1513–1527, Oct. 2011.

[9] *IEEE Std for High Rate WPANs MAC/PHY Specific. Amend. 2: Millimeter Wave Based Alternative PHY Ext.*, IEEE 802.15.3c, Oct. 2009.

[10] *IEEE Std for WLAN MAC/PHY Specific. Amend. 3: Enhanc. for Very High Throughput in the 60 GHz Band*, IEEE 802.11ad, 2014.

[11] J. G. Andrews *et al.*, "What will 5G be?" *IEEE J. Sel. Areas Commun.*, vol. 32, no. 6, pp. 1065–1082, Jun. 2014.

[12] C. A. Balanis, *Antenna Theory: Analysis and Design*. New York, NY, USA: Wiley, 1997.

[13] R. D. Yates and D. J. Goodman, *Probability and Stochastic Processes*. New York, NY, USA: Wiley, 1999.

[14] M. B. Knudsen and G. F. Pedersen, "Spherical outdoor to indoor power spectrum model at the mobile terminal," *IEEE J. Sel. Areas Commun.*, vol. 20, no. 6, pp. 1156–1169, Aug. 2002.

[15] S. Frühwirth-Schnatter, *Finite Mixture and Markov Switching Models*. New York, NY, USA: Springer-Verlag, 2006.

[16] F. Babich and M. Comisso, "Throughput and delay analysis of 802.11-based wireless networks using smart and directional antennas," *IEEE Trans. Commun.*, vol. 57, no. 5, pp. 1413–1423, May 2009.

[17] M. Abramowitz and I. A. Stegun, *Handbook of Mathematical Functions with Formulas, Graphs, and Mathematical Tables*, ser. National Bureau of Standards: Applied Mathematics, Series 55. Gaithersburg, MD, USA: National Bureau of Standards, 1964.

AUTHOR QUERY

NO QUERY.